

Monte Carlo simulation of photon scattering in x-ray absorption imaging of high-intensity discharge lamps

This article has been downloaded from IOPscience. Please scroll down to see the full text article.

2010 J. Phys. D: Appl. Phys. 43 234001

(<http://iopscience.iop.org/0022-3727/43/23/234001>)

View [the table of contents for this issue](#), or go to the [journal homepage](#) for more

Download details:

IP Address: 129.6.169.83

The article was downloaded on 28/07/2010 at 17:34

Please note that [terms and conditions apply](#).

Monte Carlo simulation of photon scattering in x-ray absorption imaging of high-intensity discharge lamps

J J Curry

National Institute of Standards and Technology, Gaithersburg, MD 20899-8422, USA

E-mail: jjcurry@nist.gov

Received 26 September 2009, in final form 11 December 2009

Published 26 May 2010

Online at stacks.iop.org/JPhysD/43/234001

Abstract

Coherent and incoherent scattering of x-rays during x-ray absorption imaging of high-intensity discharge lamps have been studied with Monte Carlo simulations developed specifically for this purpose. The Monte Carlo code is described and some initial results are discussed. Coherent scattering, because of its angular concentration in the forward direction, is found to be the most significant scattering mechanism. Incoherent scattering, although comparably strong, is not as significant because it results primarily in photons being scattered in the rearward direction and therefore out of the detector. Coherent scattering interferes with the detected absorption signal because the path of a scattered photon through the object to be imaged is unknown. Although scattering is usually a small effect, it can be significant in regions of high contrast. At the discharge/wall interface, as many as 50% of the detected photons are scattered photons. The effect of scattering on analysis of Hg distributions has not yet been quantified.

1. Introduction

The unique capabilities and promise of x-rays in diagnosing high-intensity discharge (HID) lamps have been recognized for more than half a century. As early as 1941, Carl Kenty used an x-ray tube to observe the distribution of Hg atoms in a high-pressure Hg lamp [1]; the importance of the Hg density distribution is due to its inverse proportionality to the gas temperature [2]. To the extent that the discharge is in local thermal equilibrium, the gas temperature is equivalent to the equilibrium temperature, a parameter that controls many discharge characteristics including chemical equilibrium, electrical conductivity, radiation production and thermal losses. The Hg distribution has also been obtained by interferometry [3], laser absorption [4] and laser scattering [5].

Despite Kenty's demonstration, however, x-ray imaging of the Hg distribution in HID lamps did not come into widespread use in the following years [6, 7]. The most likely reason is the difficulty in using film as a quantitative imaging detector.

Renewed interest in x-ray imaging of HID lamps began at the University of Wisconsin [8]. Since then, the technique has

been advanced at NIST [9, 10] and the Technical University of Eindhoven [11, 12]. These efforts benefitted considerably from advances in detector technologies since Kenty's original work. In particular, charge-coupled device (CCD) detectors are a linear, completely digital technology that does not have many of the negative characteristics of a film.

One aspect of x-ray absorption imaging of HID lamps that has not been addressed to date is the contribution of coherent and incoherent scattering. All analyses have proceeded under the assumption that photoelectric absorption is the only mechanism of interaction between x-rays and atoms. The relative magnitude of scattering cross-sections compared with photoelectric cross-sections would appear to make this a warranted assumption. The effect of scattering, moreover, is not easy to analyse since there are strong energy and angle dependences, as well as a finite probability of multiple interactions. Analytic descriptions of scattering can be obtained only for cases that are too simple to be of interest here.

In this paper, we give a quantitative description of x-ray scattering as it pertains to the imaging of high-intensity discharges in cylindrical arc tubes. This is achieved by utilizing

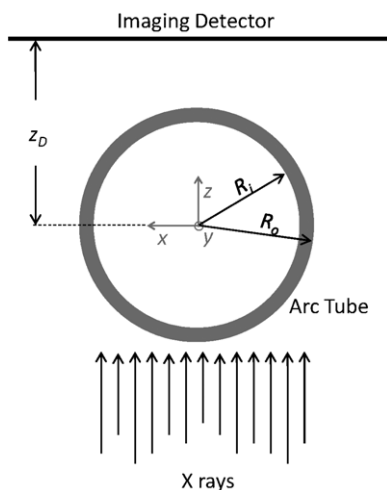


Figure 1. Our Monte Carlo code simulates the case of a parallel beam of x-rays incident on the arc tube of an HID lamp with an imaging detector behind the arc tube.

detailed Monte Carlo simulations of some interesting cases. These results indicate that scattering is most important in regions of high contrast, such as the discharge–wall interface.

2. X-ray absorption imaging

A brief description of the process of x-ray absorption imaging as applied to HID lamps is useful in understanding some of the later discussion. More thorough descriptions can be obtained from references cited above [8–12].

Figure 1 shows a typical x-ray imaging measurement. The cylindrical arc tube of an HID lamp is shown in horizontal cross-section. It is illuminated with a beam of x-rays and the transmitted photons are recorded on an array detector. The primary object of interest is the discharge that exists inside the arc tube when the HID lamp is on. This usually consists of dense Hg vapour at pressures ranging from one to several atmospheres, depending on the lamp, and temperatures of order 5000 K near the axis and of order 1300 K near the wall. The spatially dependent transmission $T(x, y)$ of the Hg vapour is obtained by taking the ratio of the x-ray shadow of the operating lamp to the x-ray shadow of the cold lamp (no discharge and Hg condensed). In this manner, absorption by the arc tube and spatial variations in the beam intensity, since they are the same in both cases, are rendered irrelevant. The projected shadow of the Hg vapour is then Abel-inverted to obtain the Hg density distribution $N(r, z)$. Implicit in this basic analysis is the assumption that the x-rays travel parallel to the beam axis and the two-dimensional projection of the three-dimensional lamp onto the array detector is direct (issues related to, e.g. phosphor conversion and optical imaging are not considered here) with unity magnification.

3. X-ray scattering

X-ray absorption imaging makes use of the intrinsic photoelectric absorption of x-rays by bound atomic electrons,

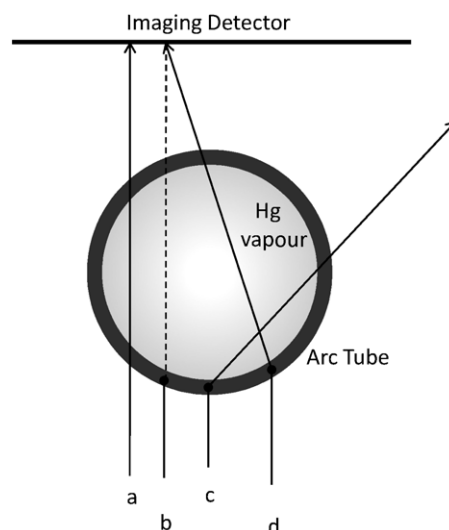


Figure 2. Possible paths of a photon incident on an arc tube filled with a Hg vapour discharge include (a) transmission without interaction, (b) photoelectric absorption, (c) scattering that prevents the photon from reaching the detector and (d) scattering that does not prevent the photon from reaching the detector, but causes it to appear as though it arrived at the detector by a different path (b).

a process in which the photon is either completely annihilated or is transmitted, unaffected, to a detector.

The same atomic electrons that lead to photoelectric absorption also lead to more complex scattering processes: coherent and incoherent scattering, sometimes referred to as Rayleigh and Compton scattering. In the range of energies of interest here, the cross-sections for these processes are generally much smaller than photoelectric cross-sections and are often justifiably ignored for the purposes of absorption imaging.

Both coherent and incoherent scattering deflect a scattered photon from its original path. The magnitude of the differential cross-section depends on the polar angle, i.e. the angle between the photon's incident and scattered wave vectors. For an unpolarized beam of photons, there is no dependence of scattering on azimuthal angle, i.e. the angle of rotation around the incident wave vector. Incoherent scattering also produces a decrease in photon energy that depends on polar angle.

Figure 2 shows some possible paths for an x-ray photon incident on a cylindrical arc tube of an HID lamp. As illustrated by path (a), there is a finite probability that a photon undergoes neither absorption nor scattering. It is transmitted, unaltered to a detector. Alternatively, a photon may be absorbed in a single event, as depicted by path (b). If a photon is scattered, the scattering angle may be large enough to prevent it from reaching the detector, as in path (c). In this case, it is experimentally indistinguishable from photoelectric absorption, path (b). If the scattering angle is small enough, as in path (d), the photon still reaches the detector, but at a location that makes it appear as though it travelled path (b). In this case, scattering gives an incorrect perception of the amount of absorption by the arc tube or by the vapour in the arc tube. It is this case that can lead to errors in quantitative absorption imaging.

Of course, a given photon may experience more than one scattering event before it is absorbed or strikes the detector. The relative frequency of multiple events, however, is low in the parameter range of interest here.

4. Monte Carlo simulation

To examine the effect of photon scattering on x-ray absorption imaging of HID lamps, we developed a Monte Carlo computer code that traces the random paths of a large number of independent photons experiencing probabilistically determined random interactions. Our code simulates a parallel beam of x-rays incident on an unjacketed HID lamp with a pixelated detector (such as a CCD detector) behind the lamp. This geometry is shown in figure 1. The dimensions of the beam, arc tube, detector and detector pixels are arbitrary, as is the distance between the lamp and the detector. The arc tube material may be chosen as either fused quartz or polycrystalline alumina. The photon energy distribution is also arbitrary. Our code does not yet include the vapour inside the arc tube.

The Monte Carlo simulation includes coherent scattering, incoherent scattering and photoelectric absorption, with multiple scattering events for each photon allowed. The differential cross-sections for coherent scattering have the form

$$\frac{d^2\sigma_c}{d\Omega} = \frac{r_e^2}{2}(1 + \cos^2\theta) F^2(E, \theta), \quad (1)$$

where r_e is the classical electron radius and $F(E, \theta)$ is the atomic form factor as a function of photon energy, E , and angle between the incident and scattered wave vectors, θ . The expression preceding the atomic form factor is the Thomson differential cross-section for scattering of unpolarized photons from free electrons. The atomic form factor modifies the Thomson cross-section by incorporating the effects of the binding potential of the atomic electrons. As photon energy decreases below the electronic binding energy, coherent scattering is increasingly suppressed at large θ . The form factors for each type of atom are taken from the tabulations of Hubbell *et al* [13]. The differential cross-section for coherent scattering of 20 keV photons by Al atoms is shown in figure 3.

The differential cross-sections for incoherent scattering have the form

$$\frac{d^2\sigma_i}{d\Omega} = \frac{r_e^2}{2} \frac{1 + \cos^2\theta + \frac{\alpha^2(1 - \cos\theta)^2}{1 + \alpha(1 - \cos\theta)}}{[1 + \alpha(1 - \cos\theta)]^2} S(E, \theta), \quad (2)$$

where $\alpha = E/E_0$ is the ratio of photon energy to electron rest energy ($E_0 = 511$ keV) and $S(E, \theta)$ is the incoherent scattering function. The factor prior to the incoherent scattering function is the Klein–Nishina formula for scattering of unpolarized photons from free electrons. The incoherent scattering function modifies the Klein–Nishina result for the effect of the atomic binding energy. For low photon energies, the binding energy tends to suppress scattering in the forward direction. The incoherent scattering functions for each type of atom are taken from the tabulations of Hubbell *et al* [13]. The differential cross-section for incoherent scattering of 20 keV photons from Al atoms is shown in figure 4.

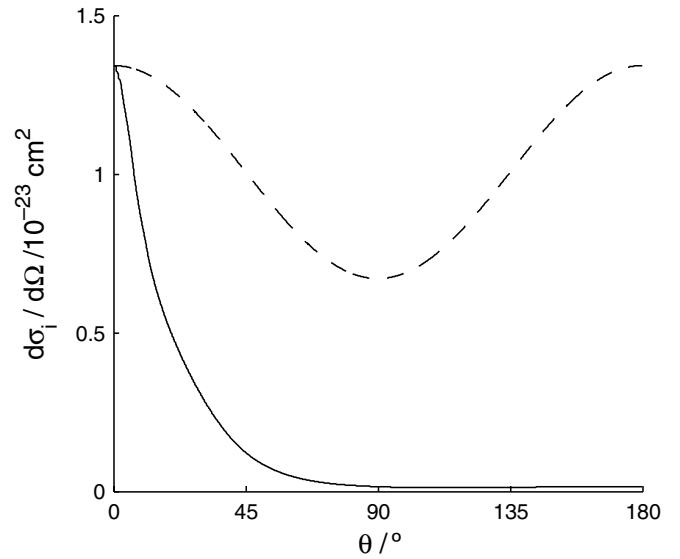


Figure 3. The Thomson differential cross-section for 20 keV photons scattering from 13 free electrons (dashed line) as a function of the polar angle θ . The differential cross-section for coherent scattering from the 13 bound electrons of Al as given by equation (1) (solid line).

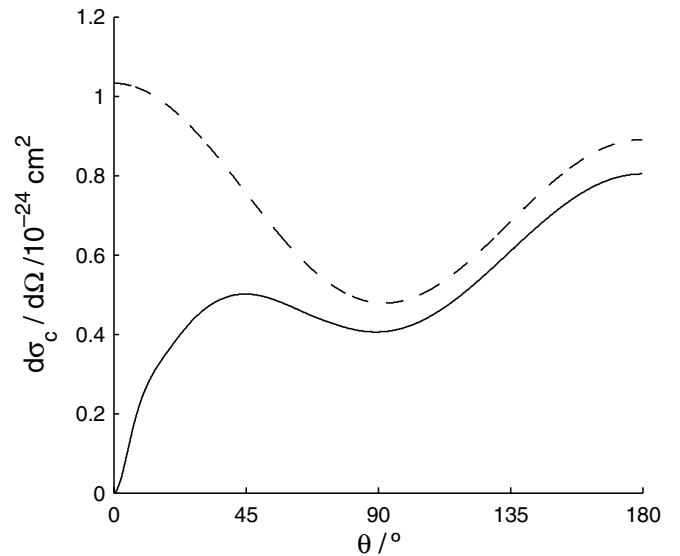


Figure 4. The Klein–Nishina differential cross-section for 20 keV photons scattering from 13 free electrons (dashed line) as a function of the polar angle θ . The differential cross-section for incoherent scattering from the 13 bound electrons of Al as given by equation (2) (solid line).

Our simulation does not include energy loss during incoherent scattering. This can be an important factor for photons undergoing multiple scattering events.

The photoelectric cross-sections are taken from Berger *et al* [14].

The photons are launched parallel to the z -axis (see figure 1) from random x_0, y_0 points within the beam cross-sectional area with equal probability. When the photon initially encounters the arc tube, initial positions $x_1 = x_0, y_1 = y_0, z_1$ are computed. A random mean free path, ℓ , is computed based on the probability of absorption or scattering and the photon

is then allowed to propagate a distance ℓ parallel to the z -axis to new coordinates $x_2 = x_1, y_2 = y_1, z_2 = z_1 + \ell$. In other words, the photon does not scatter at x_1, y_1, z_1 where it first encounters the arc tube. Rather it penetrates the arc tube at a random distance, ℓ , before scattering.

If the photon is still within the arc tube walls, an interaction process (absorption, coherent scattering, incoherent scattering with an Al or O atom in the case of PCA) is randomly determined based on the relative magnitudes of the total cross-sections. If the photon is absorbed, it is annihilated. If a scattering process occurs, a polar angle is randomly generated from the appropriate probability distribution and an azimuthal angle is randomly generated with equal probability from the interval $[0, 2\pi]$. Another mean free path is randomly generated as before and a new position x_3, y_3, z_3 is computed from the angles and mean free path. This process is continued until the photon exits the arc tube. If the trajectory of the photon causes it to strike the detector, its position on the detector (x_D, y_D) is recorded, otherwise the photon is considered lost.

At present, the interior of the arc tube ($r < R_i$) is empty and no interactions are allowed to occur there. The computed paths do correctly include propagation across the interior when they occur, with the photon re-entering the arc tube wall at the appropriate position on the other side of the interior.

The launched photons are distributed in energy according to an arbitrarily prescribed energy distribution that includes relative probabilities at a given set of fixed energies. The cross-sections, including the incoherent scattering functions and the atomic form factors, are re-computed at each energy in the distribution.

The random numbers upon which the Monte Carlo simulations are based are generated by Matlab's version 7.8 pseudorandom number generator 'rand'¹.

5. Some results

Here we examine the particular case of a polycrystalline alumina (Al_2O_3) arc tube with inner radius $R_i = 0.8$ cm and outer radius $R_o = 0.9$ cm. The detector is a square 1 mega-pixel array measuring 2.5 cm on a side. It is located at $z_D = 5$ cm (see figure 1). The beam energy distribution is a simulated spectrum of the output of a Ag-anode x-ray tube at an accelerating potential of 26 kV. A typical number of photons in a simulation is 10^9 .

The general nature of the different scattering mechanisms can be explored by using a pencil beam, i.e. one restricted to the size of a single pixel at $x_0 = 0, y_0 = 0$ (see figure 1) and observing the pattern and magnitude of scattering when all but one scattering cross-section are set to zero. Figure 5 shows a grey-scale image of the number of photons registered by the detector when we include only coherent scattering from Al atoms and photoelectric absorption from both Al and O. The position of the incident beam is shown by the black dot at the centre of the image. The vertical lines show the positions of

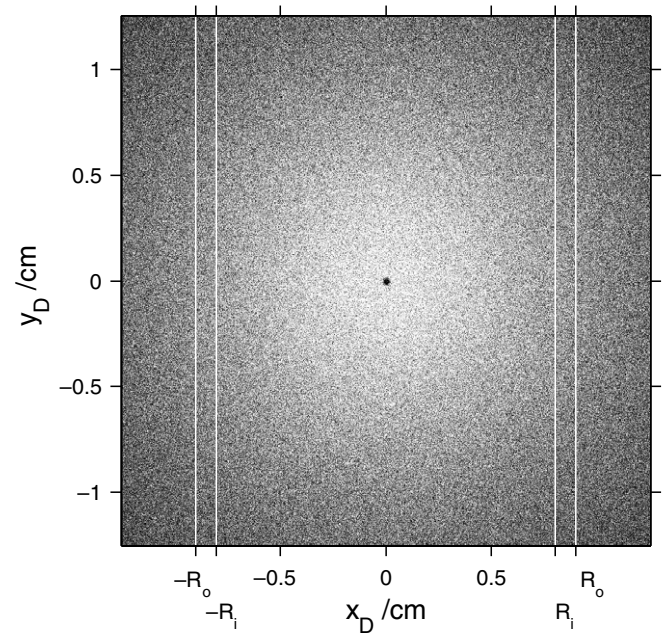


Figure 5. Grey-scale image of the photon distribution striking the detector as a result of coherent scattering from Al atoms in a PCA arc tube. The lighter pixels have recorded more photons than the darker pixels. The black dot at the centre of the image indicates the location of the incident beam. The vertical lines indicate the positions of the inner (R_i) and outer (R_o) radius of the arc tube projected onto the detector.

the arc tube walls in cross-section. Consistent with the polar angle dependence shown in figure 3, coherent scattering is concentrated in the forward direction with a solid angle that is comparable to the cone angle subtended by the detector. Of the total number of photons incident on the arc tube, only 14.4% are transmitted without interaction to the detector, 0.27% strike the detector after being scattered out of the incident beam (path (d) in figure 2) and 1.3% are scattered at angles large enough that they do not reach the detector at all. The biggest effect on the incident beam, by far, is photoelectric absorption. This is simply because the photoelectric cross-sections are substantially larger than the scattering cross-sections. (The photons scattered so they do not reach the detector necessitate a small correction to the apparent absorption cross-section.) Of greater significance is the number of scattered photons reaching the detector as a percentage of detected photons, which in this case is 1.9%.

Figure 6 plots the detected photons along the x_D -axis at $y_D = 0$ from figure 5. The scale is normalized to the total number of photons reaching the detector. Although the relative magnitude of the number of scattered photons is only $\sim 10^{-7}$ in this plot, the essential point is that the scattering distribution is broad. When a wide-area beam is used, any given pixel will see scattering contributions from all parts of the beam. These contributions add up to something on the order of 2%, the percentage discussed in the preceding paragraph for the sum of all scattered photons in the detector.

The results for coherent scattering from O atoms are similar in magnitude and nature to those discussed for Al.

The situation for incoherent scattering is considerably different from that for coherent scattering. In a simulation

¹ Identification of commercial products in this paper is done solely for the sake of clarity. Such identification implies neither recommendation nor endorsement by the National Institute of Standards and Technology, nor does it imply that the product identified is the best available for the purpose.

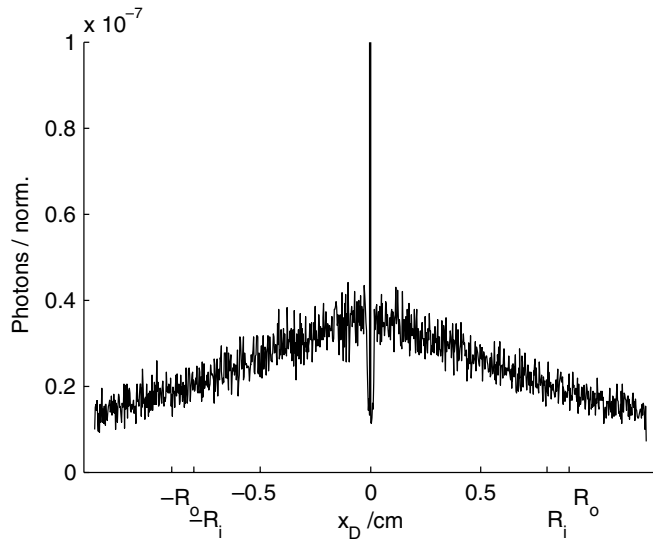


Figure 6. Plot of a horizontal slice from the image in figure 5 showing the beam peak and the broad spatial distribution of coherently scattered photons. The vertical scale is normalized to the total number of photons reaching the detector.

similar to that described above for coherent scattering, 14.8% of the incident photons are transmitted without interaction to the detector, 0.0094% strike the detector after being scattered out of the incident beam and 0.89% are scattered at angles large enough that they do not reach the detector at all. Only 0.064% of the photons reaching the detector have undergone incoherent scattering, a factor of 30 lower than for coherent scattering. The magnitudes of the integrated cross-sections for coherent and incoherent scattering by Al are comparable, but the angular dependence is different. As shown in figure 4, incoherent scattering is suppressed at small angles with most scattering events resulting in $\theta > \pi/2$. This throws most of the incoherently scattered photons outside the solid angle subtended by the detector. Incoherent scattering from O atoms in PCA gives similar results to those for Al (0.062%).

When all forms of scattering in PCA are included, 3.1% of photons reaching the detector are scattered, almost all of which is due to coherent scattering.

Looking at the more interesting situation in which the incident beam uniformly covers the entire field of view, figure 7 compares a radial profile of photons that reach the detector when no scattering mechanisms are included in the Monte Carlo simulation with a radial profile when all scattering mechanisms are included. Scattering reduces the photon flux reaching the detector, in this case on the order of 20%, depending on location.

The primary impact of scattering from the arc tube, however, is not that it changes the number of photons reaching the detector. (The practice of taking the ratio of images with and without the object of interest removes this effect since the arc tube and its scattering are present in both images.) The difficulty with scattering arises from the fact that the scattered photons carry information about regions of the imaged object that are not correlated with the position on the detector where the photon is registered (path (d) in figure 2). Therefore, the projection of the absorption shadow of Hg in the arc discharge

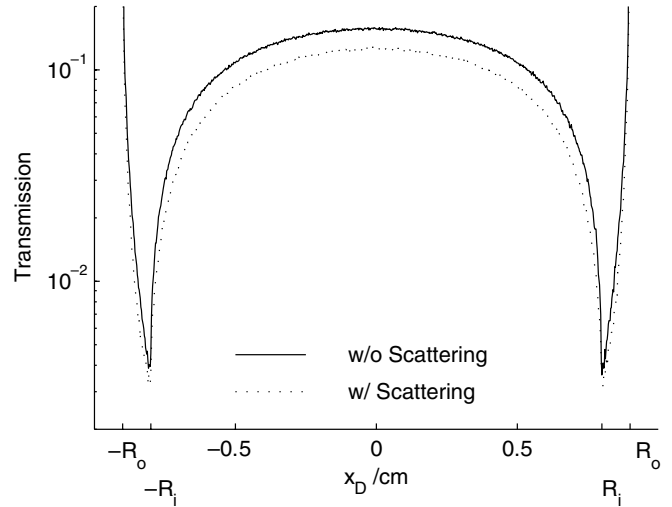


Figure 7. Radial profile of arc tube transmission in the case of an incident beam with the same dimensions as the detector and a uniform intensity distribution. The solid line comes from a simulation in which no scattering mechanisms are included. The dotted line shows results from a simulation in which all scattering processes are included.

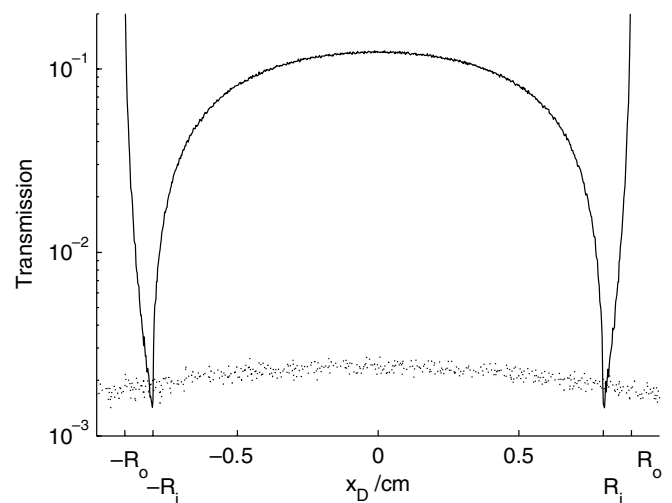


Figure 8. Radial profile of arc tube transmission in the case of an incident beam with the same dimensions as the detector and a uniform intensity distribution. Both lines are from a simulation that includes all scattering mechanisms. The solid line is derived from photons that are transmitted without scattering. The dotted line is derived from photons that reach the detector after scattering at least once.

onto the detector is not entirely a 1:1 projection. There is some scrambling of information.

Figure 8 separates the radial profile (dotted line) in figure 7 into the contribution from photons that reach the detector without scattering (solid line) and the contribution from photons that reach the detector after scattering (dots). The unscattered photons clearly show an absorption shadow that reflects the changes in the optical path length through the arc tube at different radial locations. That this profile is almost entirely the result of photoelectric absorption is made clear by the sharpness of the profile at the inner edge of the arc tube, and is consistent with the considerably larger magnitude of

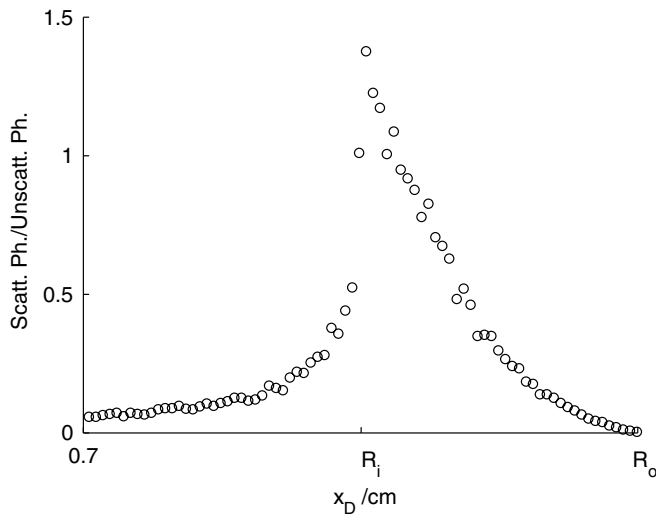


Figure 9. The ratio of scattered photons to unscattered photons (the two curves in figure 8 near the discharge/wall interface).

the photoelectric cross-section as compared with the scattering cross-sections.

The broad, featureless shape of the second contribution referred to above indicates that all the scattered photons travel nearly the same path length through the arc tube. Otherwise the profile would show strong variations in intensity due to absorption. The additional observation that the scattered photons outnumber the unscattered photons near $x_D = R_i$ makes clear that the scattered photons do not originate near $x_0 = R_i$, but instead near the centre of the beam where the path length through the arc tube is the shortest, $-0.5 < x_0 < 0.5$ cm. This is consistent with the patterns seen in figures 5 and 6 where coherently scattered photons originating at $x_0 = 0$ are scattered broadly to larger values of $|x_D|$.

The most important consequence of the preceding conclusion is that the signal detected near $x_D = R_i$ (the inner edge of the arc tube and the outer edge of the discharge) contains a substantial contribution from photons originating in the range $-0.5 < x_0 < 0.5$ cm, photons which carry information about the centre of the discharge rather than the edge of the discharge.

Figure 9 gives a closer view of the discharge–wall interface and plots the ratio of scattered photons to unscattered photons as a function of position. In the outer 250 μm of the discharge, well within the resolution of typical x-ray absorption images, the ratio is in the range 0.1–0.5 over a significant fraction of this range. The ratio does not exceed 1 except on the other side of the discharge–wall boundary, a region that is generally of little interest.

The significance of the outer region of the discharge lies with the need for an Abel inversion of the measured signal. The Abel inversion begins at the outer boundary of the discharge and propagates any errors found there into the rest of the de-convoluted profile.

The fraction of scattered photons near $x_D = 0$, although only approximately 2% of the detected photons in this case, is significant in as much as it is indicative of a limit for the precision of the measured Hg density.

6. Conclusions

The results presented here indicate that scattering by the arc tube of a HID lamp can have a significant impact on x-ray absorption imaging of the discharge. Although scattering cross-sections are small compared with photoelectric absorption cross-sections, scattering is evident in regions of high contrast such as at the discharge/arc tube boundary. Coherent scattering, which is concentrated in the forward direction, is more important than incoherent scattering.

For the case studied here, the number of scattered photons was as little as 2% of the total detected for most regions. However, in the discharge/wall interface region, scattered photons accounted for as many as 50% of the total detected. This may produce sizeable errors in the measured wall density and a portion of those errors may be propagated to other regions of the measured discharge distribution by the Abel inversion.

One way to reduce the relative number of scattered photons is to use a beam just wide enough to cover the radial extent of the discharge and just high enough to cover several rows of pixels. The field of view of such a measurement is considerably reduced, but most scattered photons will fall outside the beam area. This might reduce the number of scattered photons by one to two orders of magnitude. More sophisticated would be a collimator consisting of an array of thin tungsten sheets stacked parallel to the lamp axis and separated by a length such that only photons travelling perpendicular to the lamp axis or at small angles to it are able to reach the detector.

The actual impact of scattering on a given measurement depends on the experimental details and on the method of analysis. This is an interesting subject for further study. Future work should include the addition of an arbitrary Hg vapour distribution to the Monte Carlo model, which should make it possible to quantify the impact of scattering on measured distributions. The addition of energy loss during Compton scattering will also allow the model to be used to predict the spatial resolution of various scintillating crystals that might be used for detection. The latter improvement in the simulations would not affect the results presented here.

References

- [1] Kenty C and Karash W J 1941 *Phys. Rev.* **60** 66
- [2] Curry J J, Adler H G, Lee W K and Shastri S D 2003 *J. Phys. D: Appl. Phys.* **36** 1529
- [3] Kettlitz M, Kindel E, Schimke C and Schöpp H 1996 *Bull. Am. Phys. Soc.* **41** 1331
- [4] Schäfer R and Stormberg H-P 1986 *J. Appl. Phys.* **60** 1263
- [5] Vriens L and Adriaansz M 1974 *J. Appl. Phys.* **45** 4422
- [6] Burck V H and Dschi-yu K 1960 *Exp. Tech. Phys. (Berlin)* **8** 81
- [7] Fohl T, Kramer J M and Lester J E 1993 *J. Appl. Phys.* **73** 46
- [8] Curry J J, Sakai M and Lawler J E 1998 *J. Appl. Phys.* **84** 3066
- [9] Curry J J, Sansonetti C J and Wang J 2005 *J. Phys. D: Appl. Phys.* **38** 3086
- [10] Curry J J 2008 *J. Phys. D: Appl. Phys.* **41** 144020
- [11] Zhu X 2005 *PhD Thesis* Technische Universiteit Eindhoven Eindhoven, The Netherlands (advisors: M Haverlag and G M W Kroesen)

- [12] Nimalasuriya T 2007 *PhD Thesis* Technische Universiteit Eindhoven Eindhoven, The Netherlands (advisors: J J A M van der Mullen and M Haverlag)
- [13] Hubbell J H, Veigele W J, Briggs E A, Brown R T, Cromer D T and Howerton R J 1975 *J. Phys. Chem. Ref. Data* **4** 471
- [14] Berger M J, Hubbell J H, Seltzer S M, Chang J, Coursey J S, Sukumar R and Zucker D S 1998 available at <http://physics.nist.gov/PhysRefData/Xcom/Text/XCOM.html>